Supporting information of

"Reentrant Structural and Optical Properties of Organic–Inorganic Hybrid Metal Cluster Compound $((n\text{-}C_4H_9)_4N)_2[Mo_6Br^i_8Br^a_6]$"

Norio Saito[a,b,1], *Daiki Nishiyama*[a], *Yoshitaka Matsushita*[a], *Yoshiki Wada*[a,b], *Stéphane Cordier*[c], *Takeo Ohsawa*[a,b], *Fabien Grasset*[a,b], *Naoki Ohashi*[a,b,d,e,*]

[a] National Institute for Materials Science (NIMS), 1-1 Namiki, Tsukuba, Ibaraki 305-0044, Japan

[b] CNRS–Saint-Gobain–NIMS, IRL 3629, Laboratory for Innovative Key Materials and Structures (LINK), National Institute for Materials Science, 1-1 Namiki, 305-0044 Tsukuba, Japan

[c] Univ Rennes, CNRS, ISCR – UMR 6226, F-35000 Rennes, France

[d] NIMS-Saint-Gobain Center of Excellence for Advanced Materials, NIMS, 1-1 Namiki, Tsukuba, Ibaraki 305-0044, Japan

[e] Materials Research Center for Element Strategy (MCES), Tokyo Tech., 4259 Nagatsuta, Midori-ku, Yokohama 226-8503, Japan

[1] Present address: Department of Industrial Chemistry, Faculty of Engineering, Tokyo University of Science, 1-3, Kagurazaka, Shinjuku, Tokyo 162-8601, Japan

1. Materials and methods

1.1 Preparation of $(TBA)_2[Mo_6Br^i_8Br^a_6]$

Tetrabutylammonium molybdenum halide, $(TBA)_2[Mo_6Br^i_8Br^a_6]$, was synthesized on the basis of the method reported by Kirakci [1]. In the bromide case, $Cs_2[Mo_6Br^i_8Br^a_6]$ (5 g) was dissolved in a 50/50 ethanol (EtOH)/H_2O mixture (800 mL), and an excess of (TBA)Br (3 g) was added to the solution. Then, pristine $(TBA)_2[Mo_6Br^i_8Br^a_6]$ was precipitated. The collected precipitates were washed three times using ethanol solvent. In order to minimize impurity concentrations in the sample, we tried to recrystallize pristine $(TBA)_2[Mo_6Br^i_8Br^a_6]$ in several dehydrated solvents such as acetone (ACTN), acetonitrile (MeCN), tetrahydrofuran (THF) and a mixture of ACTN/EtOH. All operations were performed in a glovebox fulfilled with dried nitrogen gas.

1.2 Crystal structure analysis

$(TBA)_2[Mo_6Br^i_8Br^a_6]$ was crystallographically characterized using powder and single-crystal X-ray diffraction (PXRD and SCXRD) techniques. The PXRD measurement was performed with monochromatic Cu *Kα* radiation (λ = 1.5418 Å) using an Ultima III diffractometer (Rigaku). Crystal structure determination at 113, 143, and 203 K was conducted using a D8 Quest (Bruker AXS) with monochromated Mo *Kα* radiation (λ = 0.71073 Å). Also, unit cell determination at 250 and 300 K was performed with a Saturn CCD diffractometer equipped with a VariMax confocal optics (Rigaku) for a D8 Venture (Bruker AXS), with monochromated Mo *Kα* radiation. The crystal structure of $(TBA)_2[Mo_6Br^i_8Br^a_6]$ was solved using the SHELXT program [2], and SIR97 program [3] respectively, and then refined with least-square routines on F^2 using SHELXL-2014 [4] through the aid of the WinGX platform [5]. All non-hydrogen atoms were refined with anisotropic atomic displacement parameters. Atomic position of every hydrogen atom was fixed

near ideal hydrogen position determined with differential electron densities, and their displacement parameters were fixed either as 1.2 (for methylene group) or 1.5 (for methyl group) times U_{eq} of the refined values of the bonded carbon atoms.

1.3 Optical measurements

We measured photoluminescence spectra of $(TBA)_2[Mo_6Br^i_8Br^a_6]$ at different temperatures. The sample was excited with a 405 nm pulsed laser (250 fs in pulse width and 1 kHz in repetition frequency) generated from an optical parametric amplifier TOPAS Prime (Spectra Physics) excited by a titanium sapphire regenerative (Ti-Sap) amplifier Solstice (Spectra Physics). The sample temperature was maintained using a conduction type cryostat (Janis Research ST-100). Flowing cold nitrogen gas was used to cool down the sample holder in the cryostat for low temperature measurement. The luminescence was monitored using a Jovan-Ybon Triax550 spectrometer (Horiba, Ltd.) equipped with a charge-coupled device (Andor Technology).

1.4 Thermal property measurements

Differential scanning calorimetry (DSC) measurement of $(TBA)_2[Mo_6Br^i_8Br^a_6]$ was performed using a DSC 3500 (NETZSCH). An aluminum capsule containing the powder sample (5 mg) was prepared under N_2 atmosphere. The measurement was started from 103 K and then heated to 298 K with the scanning rate of 10 K/min. The heating and cooling cycle was repeated three times to examine reversibility of the thermal response.

1.5 Computational methods

Density functional theory (DFT) calculation of the solvent-inclusion compounds was performed on the basis of the method we recently reported in reference [6]. The CASTEP code [7] based on norm-conserving pseudo-potentials (NCPPs) [8−10] was utilized for all calculations. Generalized gradient approximation (GGA) optimized for solid-state compounds, i.e., the PBEsol functional [11], was used as the exchange-correlation functional for total energy calculations. Density mixing and structural relaxation schemes were the same as those of the reference [6]. The plane-wave cut-off energy was set to 1400 eV and a Monkhorst-Pack grid [12,13] (1 × 3 × 1 mesh) was employed for Brillouin zone sampling. The convergence tolerances were set to 5×10^{-5} nm for atomic displacement, 5×10^{-6} eV/atom for total energy, 0.1 eV/nm for maximum interatomic force, and 0.02 GPa for pressure.

2. Results of crystallographic characterization

Table S1. Results of the crystal structure refinements in the SCXRD measurements.

Structural formula	$(C_{16}H_{36}N)_2[Mo_6Br_{14}]$		
Formula weight / g mol^{-1}	2179.34		
Temperature / K	203(2)	143(2)	113(2)
Crystal system	Monoclinic		
Space group; Z	*P*21/*n*; 2	*P*21/*c*; 4	*P*21/*n*; 2
a / Å	13.1355(4)	22.820(3)	13.0071(10)
b / Å	11.7629(3)	11.9888(15)	11.6664(9)
c / Å	18.9747(6)	22.879(3)	19.0278(14)
β / °	90.7370(10)	111.912(4)	90.481(3)
V / Å^3	2931.57(15)	5807.2(13)	2887.3(4)
D_{cal} / g cm^{-3}	2.469	2.493	2.507
λ (Mo *Kα*) / Å	0.71073		
μ / mm^{-1}	10.810	10.914	10.976
Goodness-of-fit on F^2	1.035	0.957	1.027
Final *R*-indexes ($I > 2\sigma$)	R_1=0.0416; wR_2=0.0914	R_1=0.0643; wR_2=0.1373	R_1=0.0644; wR_2=0.1660
Final *R*-indexes (all data)	R_1=0.0730; wR_2=0.1031	R_1=0.1410; wR_2=0.1684	R_1=0.0792; wR_2=0.1770
$\Delta\rho_{max}$, $\Delta\rho_{min}$ / e Å^{-3}	0.903, –0.998	2.138, –1.829	1.825, –2.488

Table S2. Lattice parameters of $(TBA)_2[Mo_6Br^i_8Br^a_6]$ refined by the SCXRD measurements. Comparison to the reference values suggests that the present sample exhibited larger lattice volume (V/Z) at room temperature.

Temperature / K	Z	a [Å]	b [Å]	c [Å]	β [°]	V [Å^3]	V / Z [Å^3]
113	2	13.007(1)	11.666(1)	19.028(1)	90.481(3)	2887.3(4)	1443.7(2)
143	4	22.820(3)	11.989(2)	22.879(3)	111.912(4)	5807.2(1)	1451.8(1)
203	2	13.136(1)	11.763(3)	18.975(1)	90.737(1)	2931.6(2)	1465.8(1)
250	2	13.182(1)	11.824(1)	18.961(1)	90.821(4)	2955.0(4)	1477.5(2)
300	2	13.285(3)	11.914(2)	18.964(3)	90.957(9)	3001.3(9)	1500.6(5)

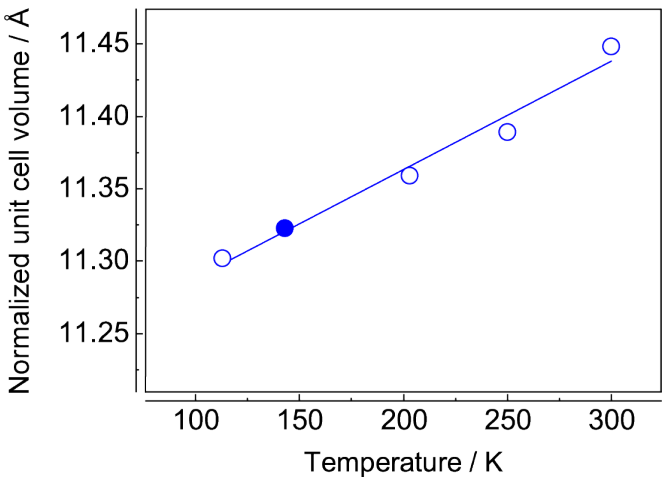

Figure S1. Temperature-evolution of normalized unit cell volume ($V^{1/3}$) of $(TBA)_2[Mo_6Br^i_8Br^a_6]$. The open and close circles indicate the unit cell volume for phase I and phase II, respectively. The unit cell volume (V) is normalized with the number of cluster unit (Z) in the unit cell. Coefficient of linear thermal expansion (α) calculated from the slope is 65.34×10^{-6} K^{-1}.

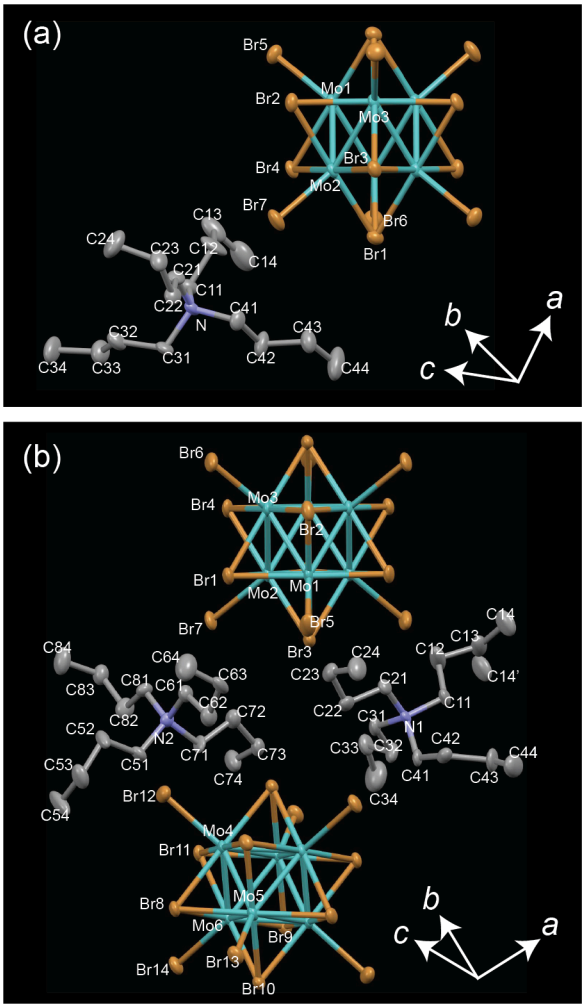

Figure S2. ORTEP diagram of $(TBA)_2[Mo_6Br^i_8Br^a_6]$ refined at (a) 113 K and (b) 143 K drawn as thermal ellipsoids at the 50% probability level. Hydrogen atoms are omitted for clarity.

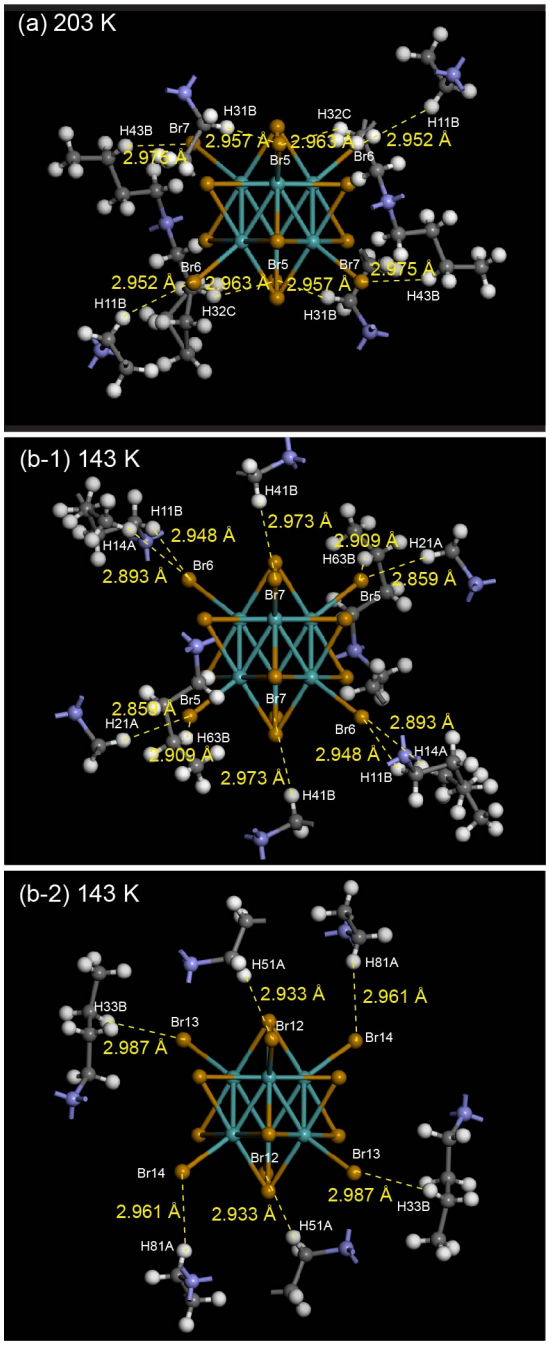

Figure S3. Coordination structures surrounding the $[Mo_6Br^i_8Br^a_6]^{2-}$ unit in $(TBA)_2[Mo_6Br^i_8Br^a_6]$ refined at (a) 203 K and (b) 143 K. In these figures, bond lengths within summation of van der Waals radius for Br and H (3.05 Å) [14] are displayed.

Table S3. Summary of averaged isotropic atomic displacement parameters (B_{iso} / Å^2) for selected crystallographic sites of $(TBA)_2[Mo_6Br^i_8Br^a_6]$ observed at 100[a], 113, 143 and 203 K.

Temperature / K	203	143	113	100[a]
Mo	2.60(4)	1.74(7)	1.67(3)	1.73(5)
Br^i	3.34(18)	2.25(15)	2.14(4)	2.23(15)
Br^a	4.43(31)	2.94(42)	2.71(18)	2.93(25)
N	3.58(13)	2.11(6)	2.03(14)	2.42(31)
C (N-CH_2-)	4.09(28)	2.32(16)	2.49(14)	2.77(21)
C (-CH_2-)	6.16(154)	3.31(97)	3.48(65)	3.90(87)
C (-CH_2-CH_3)	5.92(96)	3.29(49)	3.78(53)	4.51(82)
C (CH_3)	8.67(213)	4.85(75)	5.45(60)	5.93(99)

[a]K. Kirakci et al., Z. Kristallogr. NCS, 220, 116−118 (2005).

Table S4. Details in the B_{iso} values for $(TBA)_2[Mo_6Br^{i}_8Br^{a}_6]$ refined by the SCXRD measurements:

(a) Refined B_{iso} values for phase I observed at 113 K.

Atom (MC)	B_{iso}	Atom (TBA)	B_{iso}
Mo1	1.649	N	2.08
Mo2	1.709	C11	2.61
Mo3	1.646	C12	4.45
Br1	2.168	C13	4.26
Br2	2.167	C14	5.29
Br3	2.165	C21	2.28
Br4	2.068	C22	2.74
Br5	2.494	C23	3.07
Br6	2.706	C24	5.10
Br7	2.944	C31	2.42
		C32	3.08
		C33	4.31
		C34	4.94
		C41	2.63
		C42	3.68
		C43	3.47
		C44	6.46

(b) Refined B_{iso} values for phase I observed at 203 K.

Atom (MC)	B_{iso}	Atom (TBA)	B_{iso}
Mo1	2.551	N	3.58
Mo2	2.657	C11	4.00
Mo3	2.587	C12	8.63
Br1	3.488	C13	7.43
Br2	3.481	C14	6.15
Br3	3.048	C21	3.87
Br4	3.340	C22	4.71
Br5	4.024	C23	5.17
Br6	4.481	C24	7.63
Br7	4.789	C31	3.92
		C32	5.04
		C33	5.02
		C34	8.95
		C41	4.58
		C42	6.25
		C43	6.04
		C44	11.9

(c) Refined B_{iso} values for phase II observed at 143 K.

Atom (MC)	B_{iso}	Atom (TBA1)	B_{iso}	Atom (TBA2)	B_{iso}
Mo1	1.846	N1	2.170	N2	2.058
Mo2	1.729	C11	2.44	C51	2.20
Mo3	1.799	C12	5.80	C52	3.19
Mo4	1.734	C13	3.86	C53	3.75
Mo5	1.723	C14	4.37	C54	5.18
Mo6	1.631	C21	2.19	C61	2.56
Br1	2.192	C22	2.73	C62	3.10
Br2	2.518	C23	2.80	C63	2.96
Br3	2.402	C24	4.26	C64	5.43
Br4	2.360	C31	2.49	C71	2.27
Br5	3.614	C32	2.99	C72	2.92
Br6	3.377	C33	3.20	C73	2.60
Br7	2.680	C34	6.36	C74	3.86
Br8	2.048	C41	2.04	C81	2.39
Br9	2.186	C42	2.54	C82	3.19
Br10	2.077	C43	4.02	C83	3.11
Br11	2.234	C44	4.98	C84	4.34
Br12	2.851				
Br13	2.692				
Br14	2.420				

3. Results of optical measurements

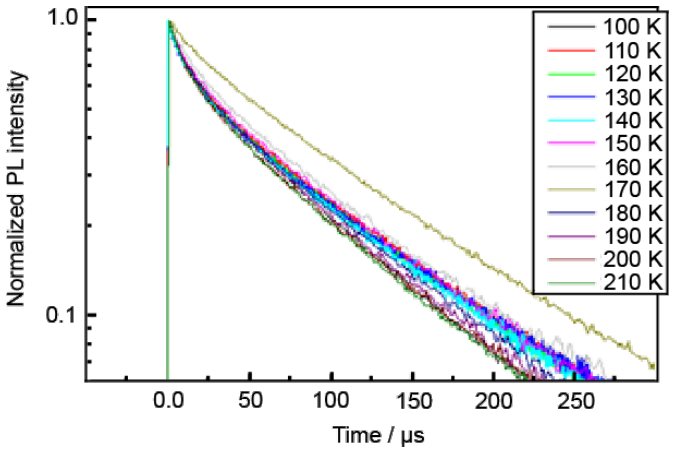

Figure S4. Temperature-variable TRPL spectra of $(TBA)_2[Mo_6Br^i_8Br^a_6]$ measured from 100 to 210 K.

Table S5. Photoluminescence lifetime (τ) of the $(TBA)_2[Mo_6Br^i_8Br^a_6]$ solid. The phase II observed at 160 K exhibited 1.7 times longer lifetime than that of the phase I observed at 100 and 210 K.

Temperature [K]	τ [μs]
100, 210	180
160	300
Reference	
100[a]	109
293[b]	66.7

[a]M. Amela-Cortes et al., J. Mater. Chem. C, 2, 1545−1552 (2014); [b]F. Grasset et al., Adv. Mater., 20, 1710−1715 (2008).

4. Results of theoretical calculations

Table S6. Lattice parameters and total energies for phase I and II of $(TBA)_2[Mo_6Br^i_8Br^a_6]$ archived by the structural relaxation calculation. The difference in both total energies is less than 0.02 eV is indicative of very comparable formation enthalpies for phases I and II.

Unit cell type	Lattice parameters					Total energy / eV
	a / Å	b / Å	c / Å	β / °	V / Å^3	
phase I (Z = 2)	13.306	12.130	19.157	90.031	3091.9	−142696.340
phase II (Z = 4)	23.061	12.240	23.156	111.62	6076.5	−285392.727

REFERENCE

[1] K. Kirakci, S. Cordier, C. Perrin, Synthesis and characterization of $Cs_2Mo_6X_{14}$ (X = Br or I) hexamolybdenum cluster halides: efficient Mo_6 cluster precursors for solution chemistry syntheses. Z. Anorg. Allg. Chem. 2005, 631, 411−416.

[2] G. M. Sheldrick, SHELXT – Integrated space-group and crystal-structure determination. Acta Crystallogr. A 2015, 71, 3–8.

[3] A. Altomare, M. C. Burla, M. Camalli, G. L. Cascarano, C. Giacovazzo, A. Guagliardi, A. G. G. Moliterni, G. Polidorib, R. Spagnac, SIR97: a new tool for crystal structure determination and refinement. J. Appl. Crystallogr. 1999, 32, 115.

[4] G. M. Sheldrick, A short history of SHELX. Acta Crystallogr. A 2008, 6, 112–122.

[5] L. J. Farrugia, WinGX suite for small-molecule single-crystal crystallography. J. Appl. Crystallogr. 1999, 32, 837–838.

[6] N. Saito, P. Lemoine, S. Cordier, Y. Matsushita, T. Ohsawa, F. Grasset, J. S. Cross, N. Ohashi, Structural and electronic properties of the metal cluster-based compounds including high concentration of solvent molecules. Z. Anorg. Allg. Chem. 2021, 647, 1−9.

[7] S. J. Clark, M. D. Segall, C. J. Pickard, P. J. Hasnip, M. J. Probert, K. Refson, M. C. Payne, First principles methods using CASTEP. Z. Kristallogr. 2005, 220, 567–570.

[8] D. R. Hamann, M. Schlüter, C. Chiang, Norm-conserving pseudopotentials. Phys. Rev. Lett. 1979, 43, 1494–1497.

[9] D. R. Hamann, Generalized norm-conserving pseudopotentials. Phys. Rev. B 1989, 40, 2980–2987.

[10] A. W. Rappe, K. M. Rabe, E. Kaxiras, J. D. Joannopoulos, Optimized pseudopotentials. Phys. Rev. B 1990, 41, 1227–1230.

[11] J. P. Perdew, A. Ruzsinszky, L. G. I. Csonka, O. A. Vydrov, G. E. Scuseria, L. A. Constantin, X. Zhou, K. Burke, Restoring the density-gradient expansion for exchange in solids and surfaces. Phys. Rev. Lett. 2008, 100, 136406 1–4.

[12] H. J. Monkhorst, J. D. Pack, Special points for brillouin-zone integrations. Phys. Rev. B 1976, 13, 5188–5192.

[13] J. D. Pack, H. J. Monkhorst, "Special points for brillouin-zone integrations"—a reply. Phys. Rev. B 1977, 15, 1748–1749.

[14] Y.-Y. Zhu, H.-P. Yi, C. Li, X.-K. Jiang, Z.-T. Li, The N—H···X (X = Cl, Br, and I) hydrogen-bonding pattern in aromatic amides: a crystallographic and ^{1}H NMR study. Cryst. Growth Des. 2008, 8, 1294–1300.